Mon. Not. R. Astron. Soc. **374,** 729–736 (2007) doi:10.1111/j.1365-2966.2006.11185.x

Parameter space study of the magnetohydrodynamic accretion flows around compact objects

Santabrata Das[1] and Sandip K. Chakrabarti[1,2]★

[1]*S.N. Bose National Centre for Basic Sciences, JD-Block, Sector III, Salt Lake, Kolkata 700098, India*
[2]*Centre for Space Physics, Chalantika 43, Garia Station Rd, Kolkata 700084, India*

Accepted 2006 October 10. Received 2006 October 9; in original form 2006 January 18

ABSTRACT

We solve the magnetohydrodynamic (MHD) equations governing axisymmetric flows around compact objects and found all possible classes of solutions for non-relativistic adiabatic accretion flows. We divide the parameter space in terms of these classes. We study the possibility of the formation of the MHD shock waves and show how the strength of the shocks depends on the flow parameters. We also show regions of the parameter space where the shock conditions are not satisfied and therefore the shocks may oscillate. These solutions are astrophysically interesting as they could give rise to quasi-periodic oscillations seen in hard X-rays.

Key words: accretion, accretion discs – black hole physics – MHD – shock waves.

1 INTRODUCTION

Magnetic field is ubiquitous in the Universe. Indeed, in many astrophysical circumstances it could even be dynamically important. Our interest in the present paper is to study the trans-magnetosonic flow properties in accretion on neutron stars (NSs) and black holes (BHs) in presence of both radial and toroidal magnetic fields. We identify all possible types of solutions and divide the region of the parameter space of the flow in terms of these types of solutions. We also study the properties of the standing magnetohydrodynamic (MHD) shock waves and especially the possibility that in a large region the shocks may be non-steady.

The study of magnetized flows in accretion/winds around stars and BHs is not new. Earlier attempts include pioneering works by Mestel (1967) and Weber & Davis (1967), who studied the first quantitative models of solar winds in the presence of magnetic fields. In the context of solar winds, the study of the trans-Alfvénic flows has been carried out by Pneuman & Kopp (1971), Okamoto (1974, 1975), Yeh (1976) and Sakurai (1985). Chakrabarti (1990) generalized the Weber–Davis model of solar wind for rotating compact stars and BHs and found a few types of solutions which are relevant to accretion and winds. Almost all the other works have been devoted to understand the effects of the accretion flows on to the magnetic field of the NS (e.g. Payne & Melatos 2004). However, there are a large number of studies in the relativistic wind and jet formation processes by different groups. Camenzind (1986, 1987) used relativistic Grad–Shafranov equations to find the outflow structures across the flow lines in a NS environment. These equations are the most relevant ones which take care of the lateral pressure of the flow tubes self-consistently. Takahashi et al. (1990) presented detailed analysis of the Alfvén point of the poloidal flow equation in full Kerr geometry. Their focus was on the poloidal flow equation for smooth trans-Alfvénic flows which can carry a negative energy influx along the field lines to the event horizon and extract energy out of the BH. They studied the solutions in the region in between two light surfaces where the injection of plasma takes place very close to the BH which then passes through the Alfvén point and the fast magnetosonic points before entering the BH. Nitta, Takahashi & Tomimatsu (1991) analytically studied the solution of general relativistic Grad–Shafranov equation and poloidal wind equation in Kerr BH geometry in the cold limit ($p = 0$). They consider the MHD conditions for the plasma inflows which pass through the Alfvén critical point. The flow is assumed to originate from the stagnation region outside the BH horizon. They find that for very rapidly spinning BHs, threading of magnetic field lines is suppressed. This may have profound implication on the evolution of magnetospheric structure around the BH. Fendt & Camenzind (1996) and Fendt (1997) numerically studied two-dimensional flow solutions in Kerr geometry by solving Grad–Shafranov equations and joined solutions across the light cylinders. From the flow topology close to the axis, it was observed that the formation of highly collimated jets from the disc boundary close to the BH is possible. Fendt & Ouyed (2004) studied ultra-relativistic outflows in the context of gamma-ray bursts. Li (1993) presented a class of self-consistent numerical solutions of outflows while Contopoulos (1994) presented an exact solution of the cold, relativistic outflows. Tsinganos et al. (1996) found a relationship of the characteristics with the critical surfaces in an outflow. Hirotani et al. (1992) showed that the magnetic field threading on to a BH has energies and angular momenta quite independent of the initial conditions (namely, the initial energy and angular momentum distribution of matter at the injection point). They showed that even when the energy injected is positive, the energy of matter may become negative on the horizon and

★E-mail: chakraba@bose.res.in

they thus showed that the energy extraction via Penrose mechanism is possible.

However, so far a complete study of the global nature of the accretion solutions (primarily the velocity versus radial distance) and their dependence on the flow parameters have not been explored. By finding the nature of the solutions, we wish to answer the following questions. (i) What are the number of sonic points in the flow and what is the dependence on parameters? (ii) What are their relative locations vis-a-vis the Alfvén point? (iii) Is a given solution closed or open (i.e. joining infinity to the BH horizon or the NS surface). A given class can be loosely referred to as a solution topology. In the present paper, we are focusing our attention to explore the dependence of the solution topology on the flow parameters such as the energy and the angular momentum of the flow. For a given pair of the Alfvén radius and the Alfvén velocity, we could identify as many as 18 types of solutions and divide the parameter space according to the nature of these solutions. Some of these topologies will allow shock formations while others will not (as we will see below). For this study, we use the so-called Paczyński & Wiita (1980) pseudo-Newtonian potential which mimics the external geometry of a Schwarzschild BH quite accurately. We also follow a non-relativistic treatment, and thus our solutions are not very accurate just outside the horizon. In any case, the radiation outside the horizon is totally redshifted away and is not observable. While Takahashi et al. (1990) and Nitta et al. (1991) concentrated on two-dimensional flows just outside the horizon, we seek solutions of flows incoming from a large distance. In this respect, the solutions we seek are complimentary to those obtained by these workers.

In many astrophysical circumstances, such as in accretion flows around stellar mass BHs and NSs, the observed spectrum extends to a very high energy ($\sim$ a few MeV). One of the ways by which such high energy radiation could be achieved is through shock acceleration of electrons (Bell 1978). These accelerated charged particles produce power-law synchrotron radiation in presence of the flow magnetic field. This has recently been used to explain the spectra of BH candidates, such as Cyg X-1 (Chakrabarti & Mandal 2006). Thus, it is advisable to look for solutions which will include the standing, oscillating or propagating shocks which will do the particle acceleration. Not only are the shocks important to energize charged particles, they can also energize low-energy photons through inverse Comptonization by the hot, post-shock (thermal and non-thermal) electrons. While the spectral characteristics would be a part of future discussions, presently we concentrate on the solutions of the MHD problem which include standing shocks and classify the parameter space especially emphasizing whether steady or non-steady shocks are allowed in the accretion flows. Though it is a matter of putting the right boundary condition (in a steady flow, at least) to distinguish whether a solution represents an outflow or a disc, and though our solutions encompass both of them, we generally concentrate on the accretion solutions in this paper. Since the sub-Alfvénic post-shock flow behaves like a boundary layer and emits most of the high energy radiation observed from the BH candidates, this is the most important region of the flow. As the flow here is non-relativistic, our treatment should be sufficiently accurate and can be readily used for computing the spectrum.

In the next section, we write the basic equations which govern the MHD flows in a pseudo-Newtonian geometry. In Section 3, we present the sonic point analysis and the sonic point conditions of the global solutions. In Section 4, we present the complete set of topologies. In Section 5, we discuss the properties of the standing shocks in detail and explore the possibility of oscillatory shock waves. Finally, in Section 6, we discuss the possible astrophysical applications and make concluding remarks.

2 BASIC EQUATIONS

We start with a stationary, axisymmetric, thin, non-self-gravitating, non-dissipative, highly conducting, adiabatic flow [$P = K\rho^{\gamma}$, P, ρ and γ being the isotropic (total) pressure, density and the constant adiabatic index, respectively] on the equatorial plane of a compact star. In case of binary systems involving BHs and NSs, it is not always essential to solve the problems using full general relativity, thanks to a few simplifying tools such as the Paczyński & Wiita (1980) potential which allows one to use the Newtonian concepts while at the same time retaining all the salient features of the space–time geometry around a compact star. As long as one is not interested in processes very close to the horizon (say, within one or two Schwarzschild radii), one may safely use this potential and obtain sufficiently accurate results. Needless to mention, the potential is used in much of the astrophysical studies around BHs quite satisfactorily.

With regard to the flow geometry, we assume that the meridional cross-section of the flow to be wedge shaped in nature. In this case, the angle subtended by the flow surface is constant throughout. It has been already shown (Chakrabarti & Das 2001) that flows of various cross-sections are 'identical' as far as the transonic properties are concerned. Thus, we chose the simpler disc geometry and we expect that the basic results will not depend on this choice.

We use the flow model to be the same as that of Weber & Davis (1967) and Chakrabarti (1990). We use the following notations. $\vartheta_{\rm r}$ and ϑ_{ϕ} are the radial and azimuthal components of velocity, $B_{\rm r}$ and B_{ϕ} are the radial and azimuthal components of magnetic field, $\phi(r) = -\frac{GM}{(r-2GM/c^2)}$ is the gravitational potential due to the compact object as prescribed by Paczyński & Wiita (1980) and Ω is the constant angular velocity of the NS or the BH. While for NS it is always valid, for a BH one has to be careful, since we are using a pseudo-Newtonian potential which mimics the non-rotating BH geometry only. However, we have verified that for the magnetic fields we are using, when Ω varies from 0 to 4, the BH spin parameter varies from 0 to 0.4 only. So the usage of the potential may be justified. We also assume the B_{θ} component to be negligible. This is justified if the flow is sufficiently thin.

MHD flow equations on the equatorial plane are as follows.

(i) The energy conservation equation:

$$E = \frac{1}{2}\vartheta_{\rm r}^2 + \frac{1}{2}\vartheta_{\phi}^2 + \frac{\gamma}{\gamma-1}\frac{p}{\rho} + \Phi(r) - \frac{B_{\phi}B_{\rm r}\Omega r}{4\pi\rho\vartheta_{\rm r}}. \quad (1)$$

(ii) The angular momentum conservation equation:

$$L = r\vartheta_{\phi} - \frac{B_{\phi}B_{\rm r}r}{4\pi\rho\vartheta_{\rm r}}. \quad (2)$$

(iii) The mass flux conservation equation:

$$\dot{M} = \rho\vartheta_{\rm r}r^2. \quad (3)$$

(iv) The radial magnetic-flux conservation equation:

$$B_{\rm r}r^2 = C_1. \quad (4)$$

(v) Maxwell's equation ($\boldsymbol{E} = -\boldsymbol{\vartheta} \times \boldsymbol{B} = \boldsymbol{0}$) for a perfectly conducting fluid on the NS surface:

$$r(\vartheta_{\rm r}B_{\phi} - \vartheta_{\phi}B_{\rm r}) = -\Omega C_1, \quad (5a)$$

where we assumed that on the surface $r = r_n$ and $\vartheta_{\rm r} = 0$. In case of a non-rotating BH, where $\vartheta_\phi = 0$ on $r = r_g$, the horizon, the above condition becomes

$$r(\vartheta_{\rm r}B_\phi - \vartheta_\phi B_{\rm r}) = r_g \vartheta_{rg} B_{\phi g} = A(\text{constant}). \tag{5b}$$

We rewrite the equations (1)–(3) as

$$\mathcal{E} = E - L\Omega = \frac{1}{2}\vartheta_{\rm r}^2 + \frac{1}{2}\vartheta_\phi^2 + na^2 + \Phi(r) - \vartheta_\phi \Omega r, \tag{6}$$

$$L = r\vartheta_\phi - C_2 r B_\phi, \tag{7}$$

$$\dot{\mathcal{M}} = a^{2n}\vartheta_{\rm r} r^2. \tag{8}$$

Here, we use the definition of adiabatic sound speed, $a^2 = \gamma P/\rho$ and

$$C_2 = \frac{B_{\rm r}}{4\pi\rho\vartheta_{\rm r}} = \frac{C_1}{4\pi\dot{M}}, \tag{9}$$

$$n = \frac{1}{\gamma - 1}, \tag{10}$$

$$\dot{\mathcal{M}} \sim K^n \dot{M} \tag{11}$$

and

$$\vartheta_\phi = \frac{\vartheta_{\rm r}L - \Omega C_1 C_2}{r\vartheta_{\rm r} - (C_1 C_2/r)} \tag{12a}$$

for NSs and

$$\vartheta_\phi = \frac{\vartheta_{\rm r}L + AC_2}{r\vartheta_{\rm r} - (C_1 C_2/r)} \tag{12b}$$

for BHs. We use $n = 3$ throughout the study.

At the Alfvén radius, $r = r_{\rm a}$ and $\vartheta_{\rm r} = \vartheta_{\rm a} = C_1 C_2/r_{\rm a}^2 = \Omega C_1 C_2/L$. The total angular momentum L and the angular velocity of the star Ω are related by $L = \Omega r_{\rm a}^2$. The flow variables in geometric units then become

$$\vartheta_{\rm a} = \frac{c}{\bar{c}}, \tag{13}$$

$$r_{\rm a} = \frac{GM}{\vartheta_{\rm a}^2 g_0}, \tag{14}$$

where c is the velocity of light, G is the gravitational constant and M is the mass of the central star. Here, $\bar{c}$ and g_0 are constants to be obtained by fixing $r_{\rm a}$ and $\vartheta_{\rm a}$ and M.

In this paper, we will use the dimensionless quantities: lengths will be measured in units of the Alfvén radius $r_{\rm a}$, velocities in units of the Alfvén speed $\vartheta_{\rm a}$ and time in units of $r_{\rm a}/\vartheta_{\rm a}$. In this case, $L = \Omega$, $B_{ra} = C_1$ and the product of the constants $C_1 C_2 = 1$. Thus for NSs, equation (12a) becomes

$$\vartheta_\phi = \frac{(\vartheta_{\rm r} - 1)\Omega r}{\vartheta_{\rm r} r^2 - 1} \tag{15}$$

and the energy expression becomes

$$\mathcal{E} = \frac{1}{2}\vartheta_{\rm r}^2 + na^2 + \frac{1}{2}\frac{(\vartheta_{\rm r} - 1)^2\Omega^2 r^2}{(\vartheta_{\rm r} r^2 - 1)^2} + \Phi(r) - \frac{(\vartheta_{\rm r} - 1)\Omega^2 r^2}{\vartheta_{\rm r} r^2 - 1}. \tag{16}$$

The corresponding equations for the BHs can be obtained using equations (5b) and (12b), respectively.

3 MAGNETOSONIC POINT ANALYSIS

In the astrophysical context, matter is accreted on a compact object either from a binary companion or from the winds of the surrounding stars. We will be interested in flows which have no viscosity so that the net angular momentum is conserved. This flow gradually moves towards the compact star and gains radial velocity due to the strong gravity. In order to study the flow properties, we first calculate the radial velocity gradient ($\mathrm{d}\vartheta_{\rm r}/\mathrm{d}r$) by differentiating equations (6) and (8) and eliminating $\mathrm{d}a/\mathrm{d}r$ which is obtained as (Chakrabarti 1990)

$$\frac{\mathrm{d}\vartheta_{\rm r}}{\mathrm{d}r} = \frac{N}{D}, \tag{17}$$

where the numerator N is given by

$$N = \vartheta_{\rm r} r\left[\left(\vartheta_{\rm r} r^2 - 1\right)^2(\vartheta_{\rm r} - 1)\Omega^2 + \left[\frac{2a^2}{r^2} - \frac{\Phi'(r)}{r}\right]\left(\vartheta_{\rm r} r^2 - 1\right)^3 + \vartheta_{\rm r}\Omega^2(1 - r^2)(\vartheta_{\rm r} - 1)\left(1 + \vartheta_{\rm r} r^2\right)\right] \tag{18}$$

and the denominator D is given by

$$D = \left(\vartheta_{\rm r}^2 - a^2\right)\left(\vartheta_{\rm r} r^2 - 1\right)^3 - \left(r^2 - 1\right)^2 \vartheta_{\rm r}^2 r^2 \Omega^2. \tag{19}$$

Here

$$\Phi_s'(r) = \frac{g_0}{(r - r_0)^2}, \tag{20}$$

where $r_0 = 2g_0/\bar{c}^2$. Equations (18) and (19) indicate that both the numerator and denominator simultaneously become zero at the Alfvén point ($r = 1$, $\vartheta_{\rm r} = 1$). Apart from the Alfvén point, they may vanish at some other points also. These points are called the critical points and are commonly known as the magnetosonic points in the context of MHD study. At these points, the flow velocity becomes equal to the speed of the magnetosonic waves. At the outer edge of the accretion disc, the radial velocity of the flow remains sub-magnetosonic as the flow velocity is very small. For a NS accretion, since on the star surface the radial velocity is again zero, the matter will accrete submagnetosonically. Thus, the flow may or may not become super fast- or slow-magnetosonic before touching the star surface. For a BH accretion, however, the inner boundary condition is different but unique. Here, the flow enters with the velocity of light, while the speed of the magnetosonic wave is never so high due to causality reason. Thus, the matter must cross the horizon super-magnetosonically. This means that the flow must cross the magnetosonic point at least once before entering into the BH.

4 BEHAVIOUR OF THE PARAMETER SPACE AND THE SOLUTION TOPOLOGIES

We now divide the parameter space into various regions depending on the nature of the solution topologies in NS and BH accretion. In Fig. 1, we show this division in energy and angular momentum plane. Accretion flow solution in BH and NSs differs only through inner boundary conditions. Thus, for a pair of flow parameters, the curves representing the solutions (velocity versus distance) remain the same, and only depend on the flow parameters. In other words, Fig. 1 is independent of the nature of the compact object. For a BH accretion, the inner boundary condition is that the flow must be super-Alfvénic on the horizon, while for a NS accretion, the radial velocity must vanish. This will distinguish between the branches relevant for BHs and NSs. For each topology, we need to put a boundary condition to decide whether the solution is for BH or for a

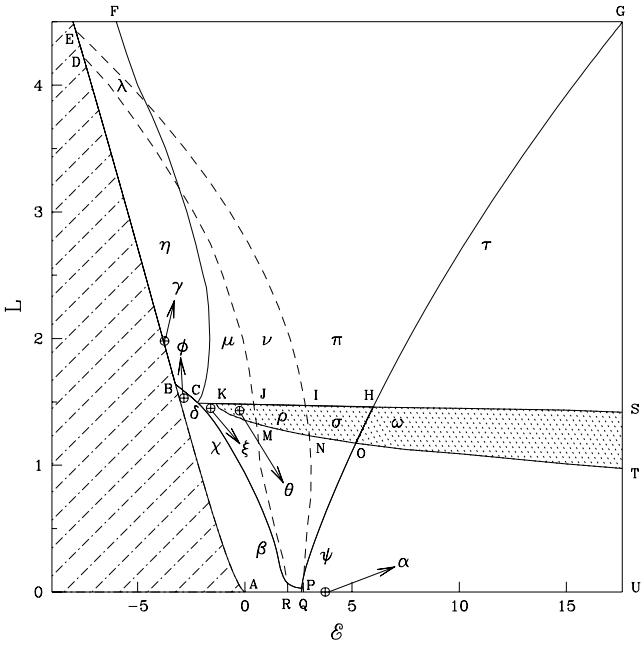

Figure 1. Division of the parameter space according to the solution topologies. See text for more details.

NS. The curves ADE and PG are obtained using theoretical considerations alone, while others would come only from the numerical solutions.

4.1 Curve ADE

This curve is obtained for the special case where the radial velocity $\vartheta_r = 0$ at all the sonic points. In this case, equations (18)–(19) give rise to

$$r^3 + 2r_0r^2 + r_0^2r - \frac{g_0}{\Omega^2} = 0. \tag{21}$$

We incorporate the above condition in the energy conservation equation and obtained a simplified relation as

$$\mathcal{E} = -\frac{g_0}{r - r_0} - \frac{\Omega^2 r^2}{2}. \tag{22}$$

For a given angular momentum L, the location of the sonic point can be obtained from equation (21), and the energy of the flow is obtained from equation (22). Below the curve ADE, no solution is possible.

4.2 Curve PG

This curve is obtained by putting ($\vartheta_r = 1$) the other extreme case. The flow velocity at the magnetosonic point (occurring at $r < 1$) is exactly the same as the Alfvén velocity. Setting $\vartheta_r = 1$ in equations (18)–(19), we get

$$2(1 - \Omega^2)r^4 - [4r_0(1 - \Omega^2) + g_0]r^3 + 2\left[r_0^2(1 - \Omega^2) - 1\right]r^2 + (4r_0 + g_0) - 2r_0^2 = 0. \tag{23}$$

Now, we put $\vartheta_r = 1$ in the energy equation and obtain

$$\mathcal{E} = \frac{1}{2} + \frac{nr\Phi'}{2} + \Phi. \tag{24}$$

For a given L, equation (23) gives the location of the magnetosonic point. The corresponding energy of the flow is obtained from equation (24).

Other curves are obtained using the following considerations. Following Chakrabarti (1990), let us first denote the magnetosonic points with (i) $r < 1$, $\vartheta_r < 1$, (ii) $r < 1$, $\vartheta_r > 1$, (iii) $r > 1$, $\vartheta_r < 1$ and (iv) $r > 1$, $\vartheta_r > 1$ as 'Bondi-like Slow', 'Bondi-like fast', 'rotational slow' and 'rotational fast', respectively. The reason for giving them these names is this: the inner-most magnetosonic point occurs even with negligible rotational motion, i.e. in spherical or quasi-spherical Bondi-like flows. The outer magnetosonic points occur only because of rotation.

Our findings regarding the parameter space are follows. (i) The Bondi-like slow magnetosonic points exist in a region surrounded by the boundary PBEGHP. (ii) The Rotational-slow magnetosonic points exist in a region surrounded by the boundary ABCFGUA (for $L > 0$). (iii) The Rotational-fast magnetosonic points exist in a region surrounded by the boundary RDEQR and $L = 0$ and $\mathcal{E} > 0$. (iv) The Bondi-like fast magnetosonic points exist in a region surrounded by the boundary QGUQ (for $L > 0$). (v) The region surrounded by the boundary SKTS and shaded by the dots indicates the region in which magnetosonic shocks may form. (vi) The region of the parameter space shaded by the dot–dashed lines denotes the forbidden region for the flow solution. (vii) The region surrounded by the boundary PCKOTUQP has the solution topologies to form magnetosonic shocks, but the standing shocks do not form as the shock conditions are not satisfied.

The entire parameter space spanned by the energy and the angular momentum of the flow is subdivided further according to the nature of the solutions. We scanned the complete parameter space to look for new topologies and obtained 18 distinct types of solutions as shown in Fig. 2. Each solution type is identified by a Greek alphabet $\alpha, \beta, \ldots$, etc. These Greek alphabets in the parameter space denote the regions of the parameters for which the solutions are drawn. In Fig. 2, the Bondi-like (slow/fast), rotational slow and rotational fast magnetosonic points are denoted by r_1, r_2 and r_3, respectively. When $L = 0$, since $\vartheta_\phi = B_\phi = 0$, the solutions become identical to Bondi type. Note that there are several curves in each plot, all are drawn for the same flow parameters. Only the trans-magnetosonic curve which connects infinity with the horizon (with or without shock, see below) will be a complete solution for a BH provided it is also super-magnetosonic in the inner boundary. For a NS, the appropriate branch (which is submagnetosonic on the star surface) should be chosen.

We wish to emphasize that even though the usage of the Paczyński–Wiita potential allows us to follow solutions with relativistic velocity, the treatment will be incorrect in regions right outside the horizon, since we are not treating the problem relativistically. A proper treatment would perhaps shift the locations of the inner sonic points one way or the other, but the topologies are not expected to be different.

5 STANDING MHD SHOCKS

It is clear that since the inner boundary condition of a BH accretion is super-magnetosonic, the classes of solutions which are endowed with only one magnetosonic point cannot have shocks in accretion flows on a BH. However, we note in Fig. 2 that there are several regions of the parameter space in which the solution may have two magnetosonic points. If the shock conditions are fulfilled in between these two points, then an accretion flow, after passing through the rotational-slow magnetosonic point, will pass

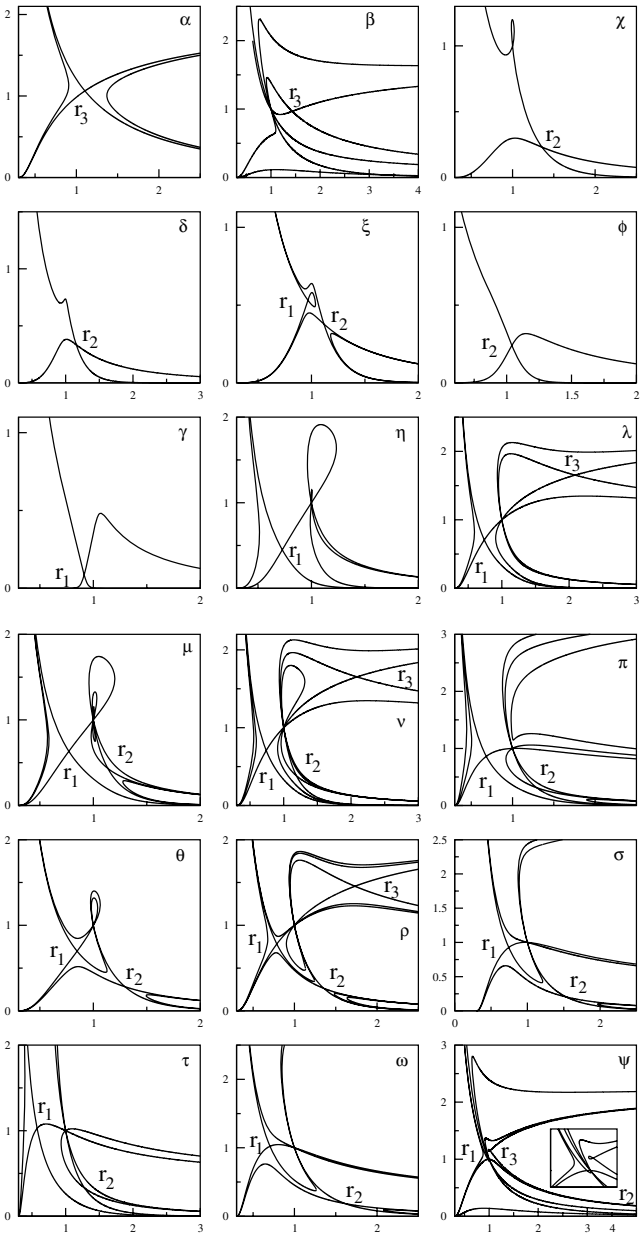

Figure 2. Solutions of the MHD flows for various (E, L) pairs of conserved parameters. Greek alphabets mark different types of solutions drawn with parameters from different regions marked in Fig. 1. Along horizontal axis is the radial distance in units of the Alfvén radius and along vertical axis is the radial velocity in units of the Alfvén velocity. The magnetosonic points are labelled as r_1, r_2 and r_3, respectively. The solution of type α is obtained when L is zero, and the solution becomes similar to a Bondi solution. Out of several curves in each plot, a complete solution is the one which connects, through shock or not, infinity with the horizon or the star surface.

through a (slow) shock and subsequently pass through a Bondi-like slow magnetosonic point. Even when the shock conditions are notionally fulfilled, one has to verify that the entropy at the inner magnetosonic point is always higher compared to that at the outer magnetosonic point. The difference in entropy is guaranteed to be generated at the shock (through turbulence, for instance) if the shock conditions are fulfilled. The shock conditions are as follows.

(i) The total energy flux is conserved across the shock:

$$\frac{1}{2}\vartheta_{r+}^2 + \frac{1}{2}\vartheta_{\phi+}^2 + na_+^2 - \vartheta_{\phi+}\Omega r_+ = \frac{1}{2}\vartheta_{r-}^2 + \frac{1}{2}\vartheta_{\phi-}^2 + na_-^2 - \vartheta_{\phi-}\Omega r_-.$$

(ii) The total mass flux is conserved:

$$\rho_+\vartheta_{r+} = \rho_-\vartheta_{r-}.$$

(iii) The radial momentum is balanced:

$$p_+ + \rho_+\vartheta_{r+}^2 + \frac{B_{\phi+}^2}{8\pi} = p_- + \rho_-\vartheta_{r-}^2 + \frac{B_{\phi-}^2}{8\pi}.$$

(iv) The transverse momentum is balanced:

$$\rho_+\vartheta_{r+}\vartheta_{\phi+} - \frac{B_{r+}B_{\phi+}}{4\pi} = \rho_+\vartheta_{r-}\vartheta_{\phi-} - \frac{B_{r-}B_{\phi-}}{4\pi}.$$

(v) The radial magnetic flux is conserved:

$$B_{r+} = B_{r-}.$$

(vi) The field equation is independently satisfied on either side of the shock:

$$\vartheta_{\phi+}B_{r+} - \vartheta_{r+}B_{\phi+} = \vartheta_{\phi-}B_{r-} - \vartheta_{r-}B_{\phi-}.$$

In Fig. 3, we provide examples of the solutions obtained using parameters from the region SKTS, which possess standing, slow-magnetosonic shocks. We chose the parameters $\vartheta_a = 10^{10}$ cm s^{-1} and $r_a = 10^7$cm while the central mass was chosen to be $10\,M_\odot$ for illustration purpose. In this unit, the Schwarzschild radius is 0.296. The parameter $(\mathcal{E}, L)$ pairs are (i) 0.0, 1.4, (ii) 1.5, 1.45, (iii) 4.0, 1.3 and (iv) 6.0, 1.3, respectively, and the shock locations are $r_s = 1.034, 1.153, 1.056, 1.09$, respectively. These locations are thus merely about $3.5r_g$ away. The standing shock locations are also marked with the vertical dashed lines. The single arrowed curve represents the solution towards a BH. The double-arrowed curve, which is sub-Alfvénic throughout the flow, is appropriate for a NS accretion without a shock transition. The triple-arrowed vertical line (dash–dotted) indicates a typical shock transition at the boundary of the NS. Since we are not considering relativistic treatment, the quantities just outside of the horizon would not be accurate. On the other hand, radiations from regions right out of the horizon would be redshifted away and would not be astrophysically relevant. From the astrophysical point of view, the post-shock region, where the radial flow is slowed down and the flow becomes hotter, is the most important one as this is the place where hard X-rays are generated. The major observational findings are thus the outcome of various physical processes in the post-shock region which is a few Schwarzschild radii away. Since this region is submagnetosonic and highly subrelativistic, our pseudo-Newtonian approach should be adequate in this region.

In Fig. 4, we show how the number of magnetosonic points is determined for a given pair of parameters. The procedure is to draw two sets of contours in a plane spanned by the sonic point location and the sonic point velocity. One set is for the specific energy and the other set is for the specific angular momentum, and see where and how many times the same pair of contours intersect. For instance, if we take Case (ii) above, three magnetosonic points are found to be present. Among them r_1 is Bondi-like slow, r_2 is rotational slow and r_3 is rotational fast magnetosonic points. The solid curves are for $\mathcal{E} = 1.5$ and the dashed curves are for $L = 1.45$. These curves intersect at three points r_1, r_2 and r_3 which are the magnetosonic points for this case. These contours are drawn using equations (18)–(19) given above.

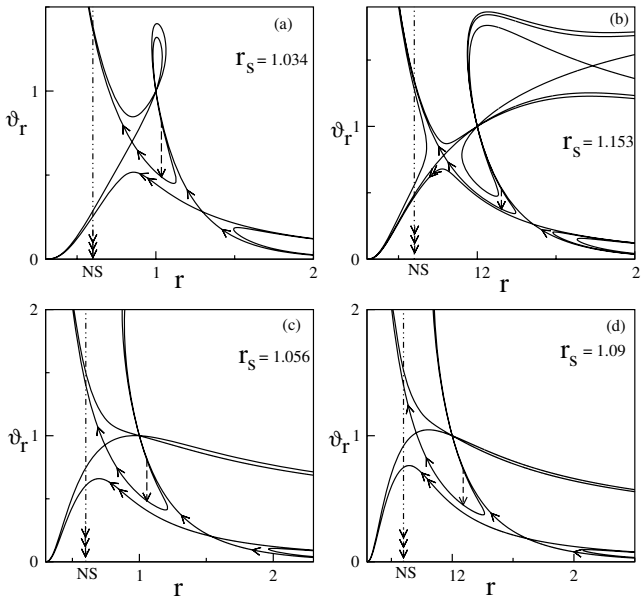

Figure 3. Four examples of solution topologies with the standing MHD shock waves. The parameters (E, L) used are (i) 0.0, 1.4, (ii) 1.5, 1.45, (iii) 4.0, 1.3 and (iv) 6.0, 1.3, respectively. The shock locations are written in box.

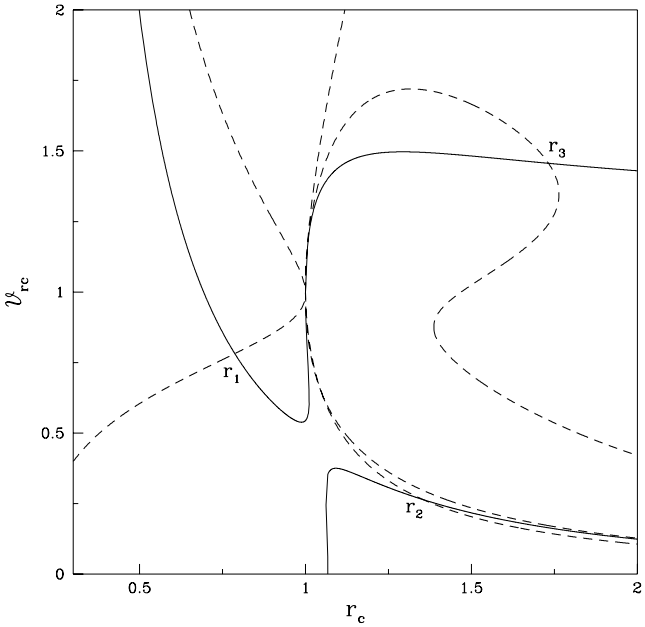

Figure 4. Intersections r_1, r_2 and r_3 of the $E = 1.5$ (solid) and $L = 1.45$ (dashed) curves in the critical point (r_c) versus critical velocity (ϑ_{rc}) plane represent the actual number and locations of the critical points for this pair of flow parameters.

In Fig. 5, we show how the strength of the shock (defined by the ratio of the post-shock Mach number and the pre-shock Mach number) depends on the flow parameters (solid curves). The angular momenta used are, from the left- to the right-hand side, 1.45, 1.40, 1.35, 1.30, 1.25 and 1.20, respectively. For a given energy of the flow, the strength of the shock decreases as the flow angular momentum increases. On the other hand, for a given angular momentum, shock strength gradually increases with the decrease of the flow energy.

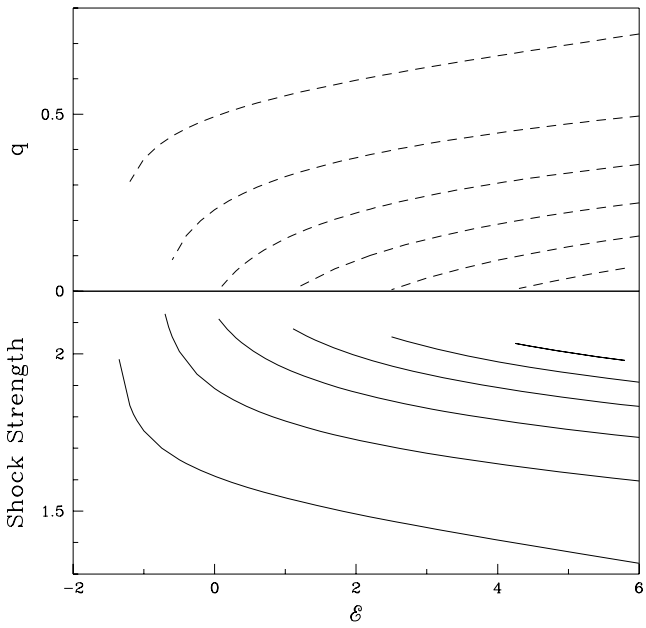

Figure 5. Variation of the shock strength with the energy and angular momentum is shown in the lower panel (solid curves), and the ratio of post-shock to pre-shock values of the azimuthal components of the magnetic field (dashed curves) is shown in the upper panel. The angular momenta used are, from the left to the right-hand side, 1.45, 1.40, 1.35, 1.30, 1.25 and 1.20, respectively. For a given angular momentum, the shock strength decreases with energy. Switch shock occurs for parameters for which $q = 0$ is reached.

There is a cut-off in the shock strength for each angular momentum as the shock ceases to exist there. We also show in dashed curves how the ratio (post-shock quantity divided by the pre-shock quantity) of the azimuthal components of the magnetic fields behaves for the same set of parameters. As the ratio approaches zero, we achieve the limit $q = 0$ for switch shocks which occur at increasingly higher energy for lower angular momenta. It is to be noted that the submagnetosonic branch cannot pass through any shocks, let alone the so-called switch-shocks. Thus, the inner boundary condition of matter rotating with the star is always satisfied.

It may be instructive to study how various flow parameters jump at the shock locations. In Fig. 6, we present the variations of the flow density ρ, the azimuthal component of the velocity (ϑ_ϕ), the azimuthal component of the magnetic field (B_ϕ) and the radial component of the velocity ϑ_r. At the shock ($r_s = 1.153$), ϑ_ϕ drops by more than 20 per cent, B_ϕ drops by over 40 per cent, ϑ_r drops by about 30 per cent, while the density goes up by more than 40 per cent.

In order to have a 'feel' for some important parameters in physical units, we note that for $r_a = 10^7$ cm and $\vartheta_a = 10^{10}$ cm s^{-1}, the unit of time is $r_a/\vartheta_a = 10^{-3}$ s. Thus, the unit of specific energy $\mathcal{E}$ is 10^{20} cm^2 and the unit of Ω is 10^3 s^{-1}. For a BH accreting with specific energy (sum of kinetic, thermal and gravitational) of matter of around 10 per cent of the rest mass, we have $\mathcal{E} = 0.9$ and $\Omega = 6.28$. The physical difference in these two cases will be that for a BH, the mass may be $M_{BH} = 10\,M_\odot$, and hence the location of the Alfvén radius would be at around $r_a = 3.3r_g$. However, for a NS, the mass may be very low, $M \sim 1\,M_\odot$, and hence the Alfvén radius is at $r_a = 33r_g$, very far away from the star surface. For a given set of dimensionless flow parameter, the solution branches being different, the physical quantities on the branch leading to a BH horizon and to a NS surface would be different. In Table 1, we compare the flow

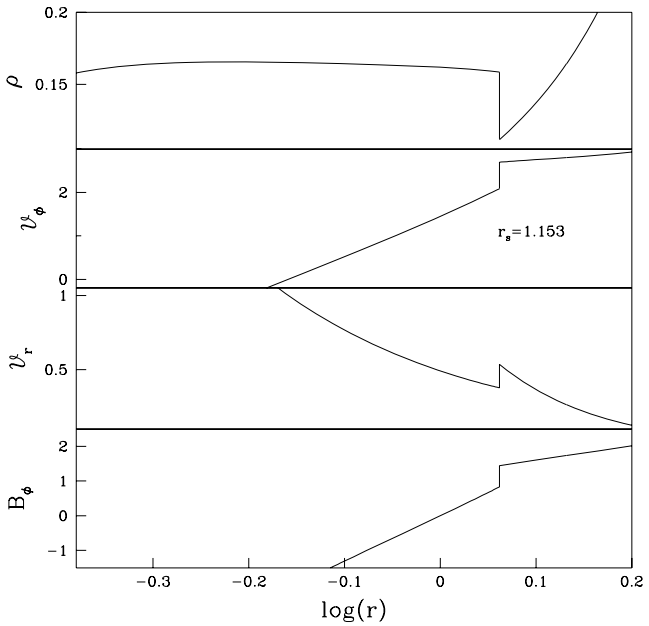

Figure 6. Variations of the flow density ρ, azimuthal component of the velocity (ϑ_ϕ), radial component of velocity $\vartheta_{\rm r}$ and azimuthal component of the magnetic field (B_ϕ) across a slow-magnetosonic standing shock in an accretion flow.

Table 1. Comparison of the flow variables at the shock for a flow around a BH of mass $10\,{\rm M}_\odot$ with that around a NS of mass $1\,{\rm M}_\odot$

	E	Ω	ϑ_{r-}	ϑ_{r+}	na_-^2	na_+^2	Δna^2	ΔT (^{o} K)
BH	0.0	1.4	0.8309	0.4894	2.2330	2.7314	0.4984	7.55104E+10
NS	0.0	1.4	0.2872	0.0	4.6913	4.7473	0.0560	8.48432E+08
BH	1.5	1.45	0.5362	0.3775	3.7825	4.2966	0.5141	7.78891E+10
NS	1.5	1.45	0.4871	0.0	6.1003	6.2730	0.1727	2.61650E+9
BH	4.0	1.3	0.8195	0.4844	5.2323	6.5674	1.3351	2.02275E+11
NS	4.0	1.3	0.7456	0.0	8.2914	8.6987	0.4073	6.17083E+9
BH	6.0	1.3	0.7448	0.4512	6.9196	8.5496	1.6300	2.46954E+11
NS	6.0	1.3	0.9192	0.0	10.0412	10.6988	0.6576	9.96302E+9

variables at the shock for a flow around a BH of mass $10\,{\rm M}_\odot$ ($r_{\rm a}$ and $v_{\rm a}$ same as above) with that around a NS of mass $1\,{\rm M}_\odot$ ($r_{\rm a}$ same as above and $\vartheta_{\rm a} = 3.3 \times 10^9$ cm s^{-1} so as to keep g_0 and $\bar{c}$ fixed).

In Fig. 7, we show the nature of the velocity and magnetic field vector of a typical accretion flow around a NS and a BH on the equatorial plane. In the case of a NS accretion, we have chosen only the submagnetosonic flow and the matter is seen to wind up while rotating along with the star. In the case of the BHs, on the other hand, ϑ_ϕ is identically zero on the horizon and B_ϕ also disappears. At the outer edge of the disc, matter with significant angular momentum starts spiralling towards the central object due to strong gravity. In the case of neutron star, radial flow velocity gradually dominates over the azimuthal velocity as matter moves inward. But, close to the

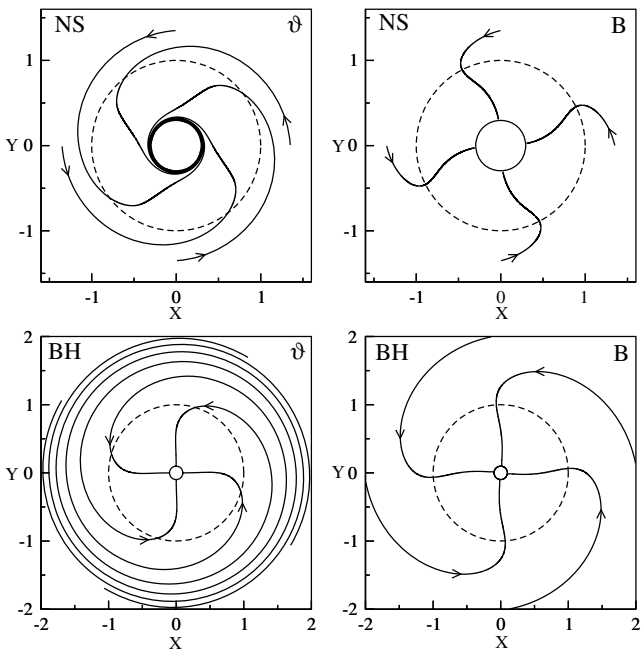

Figure 7. The nature of the velocity and magnetic fields in accretion flows around a star (upper panels denoted by NS) and a BH (lower panels denoted by BH) in the equatorial plane. For the star, only the sub-Alfvénic branch has been chosen where the inner boundary conditions are satisfied on the surface. On BHs, the trans-Alfvénic branch was chosen to satisfy the boundary condition on the horizon. The dashed circle is drawn at the Alfvén surface.

star surface, the radial velocity becomes negligible and the matter acquires the angular velocity of the star on the stellar surface. On the other hand, in the case of a BH, the radial velocity of matter increases monotonically as it proceeds towards the BHs and crosses the horizon radially.

The nature of the magnetic field, in both the cases, is quit similar. The radial component of magnetic field dominates over the azimuthal component of magnetic field as matter proceeds towards the central object. This is not surprising, since in the present study radial component of magnetic field varies with inverse square of the radial distance.

The dashed circle represents the Alfvén radius ($r = 1$) and the solid circle near the centre represents one Schwarzschild radius ($r = r_g$) where the Paczyński–Wiita potential is singular. For NS, $r_{\rm a} = 10^7$ cm and $\vartheta_{\rm a} = 10^{10}$ cm s^{-1}, hence $r_g = 0.296$. The energy and angular momentum parameters are 1.5 and 1.45, respectively. For BHs, $r_{\rm a} = 3 \times 10^7$ and $\vartheta_{\rm a} = 10^{10}$ cm s^{-1}, which yields $r_g = 0.0988$. Here, the energy and angular momentum parameters are 0.7 and 0.5, respectively. For a realistic star, the surface is larger than $r \gtrsim 3r_g$ and the inner boundary condition is to be chosen at the surface.

6 CONCLUDING REMARKS

In this paper, we have presented all possible topologies of a MHD, quasi-equatorial, adiabatic flow around compact objects. We divided the entire parameter space spanned by specific energy and angular momentum of the flow according to different types of the flow topologies. We show that in a significant region (bounded by SKTS in Fig. 2) the flow satisfies the standing shock conditions. In another region (bounded by PCKOTUQP), all the required magnetosonic points are present to form a shock, but the shock conditions

themselves are not satisfied. In Chakrabarti (1990), it was shown that for an accretion flow, the inner magnetosonic points are endowed with higher entropy than the outer magnetosonic points and we find that this is always true. Thus, a perturbed flow, even when the shock condition is not satisfied, is likely to pass through a shock which will then oscillate as in the case of the hydrodynamic flow (Ryu, Chakrabarti & Molteni 1997). Since a post-shock region is hot, the electrons in this region would inverse Comptonize low-energy photons from the cooler, pre-shock flow either from the Keplerian disc or from the synchrotron radiation (emitted in presence of magnetic fields). These photons are then re-emitted as the hard X-rays. This has been shown to be the case for non-Magnetic flow (Chakrabarti & Titarchuk 1995; Chakrabarti & Mandal 2006). Moreover, since the Alfvén radius could be close to the BH depending on the magnetic field, a MHD shock could occur close to the BH and thus the oscillation period, which is close to the infall time-scale (Molteni, Sponholz & Chakrabarti 1996; Chakrabarti, Acharyya & Molteni 2004), is likely to be very small. This could give rise to the high-frequency quasi-periodic oscillations of hard X-rays as observed in several BH candidates. Thus, we expect that the spectral and timing properties of BH candidates could be modelled satisfactorily with magnetized, shocked accretion flows. In future, we plan to carry out numerical simulations to verify some of these assertions. We also plan to extend our work with various cooling processes and viscous heating processes. In the context of hydrodynamic flows, such processes would generally shift the region of the parameter space where shocks are possible (Das & Chakrabarti 2004).

ACKNOWLEDGMENTS

This work is partly supported by a project (Grant No. SP/S2/K-15/2001) funded by Department of Science and Technology (DST).

REFERENCES

Bell A. R., 1978, MNRAS, 182, 147
Camenzind M., 1986, A&A, 162, 32
Camenzind M., 1987, A&A, 184, 341
Chakrabarti S. K., 1990, MNRAS, 246, 134
Chakrabarti S. K., Acharyya K., Molteni D., 2004, A&A, 421, 1
Chakrabarti S. K., Das S., 2001, MNRAS, 327, 808
Chakrabarti S. K., Mandal S., 2006, ApJ, 642, L49
Chakrabarti S. K., Titarchuk L. G., 1995, ApJ, 455, 623
Contopoulos J., 1994, ApJ, 432, 508
Das S., Chakrabarti S. K., 2004, IJMPD, 13, 1955
Fendt C., 1997, A&A, 319, 1025
Fendt C., Camenzind M., 1996, A&A, 313, 591
Fendt C., Ouyed R., 2004, ApJ, 608, 378
Hirotani K., Takahashi M., Nitta S., Tomimatsu A., 1992, ApJ, 386, 455
Li Z.-Y., 1993, ApJ, 415, 118
Mestel L., 1967, in Sturrock P. A., ed., Plasma Astrophysics. Academic Press, New York
Molteni D., Sponholz H., Chakrabarti S. K., 1996, ApJ, 457, 105
Nitta S., Takahashi M., Tomimatsu A., 1991, Phys. Rev. D, 44, 2295
Okamoto I., 1974, MNRAS, 166, 683
Okamoto I., 1975, MNRAS, 173, 357
Paczyński B., Wiita P. J., 1980, A&A, 88, 23
Payne D. J. B., Melatos A., 2004, MNRAS, 351, 569
Pneuman G. W., Kopp R. A., 1971, Sol. Phys., 18, 258
Ryu D., Chakrabarti S. K., Molteni D., 1997, ApJ, 470, 460
Sakurai T., 1985, A&A, 152, 121
Takahashi M., Nitta S., Tatematsu Y., Tomimatsu A., 1990, ApJ, 363, 206
Tsinganos K., Sauty C., Surlantzis G., Trussoni E., Contopoulos J., 1996, MNRAS, 283, 811
Weber E. J., Davis L. Jr, 1967, ApJ, 148, 217
Yeh T., 1976, ApJ, 206, 768

This paper has been typeset from a TEX/LATEX file prepared by the author.